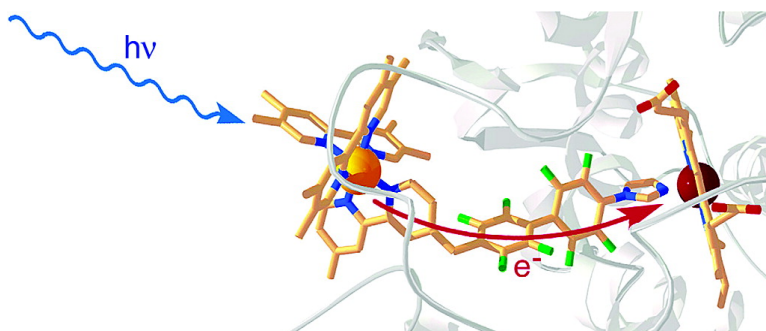## Article

Nanosecond Photoreduction of Cytochrome P450cam by Channel-Specific Ru-diimine Electron Tunneling Wires

Alexander R. Dunn, Ivan J. Dmochowski, Jay R. Winkler, and Harry B. Gray

More About This Article

Additional resources and features associated with this article are available within the HTML version:

- Supporting Information
- Links to the 5 articles that cite this article, as of the time of this article download
- Access to high resolution figures
- Links to articles and content related to this article
- Copyright permission to reproduce figures and/or text from this article

View the Full Text HTML

Nanosecond Photoreduction of Cytochrome P450cam by Channel-Specific Ru-diimine Electron Tunneling Wires

Alexander R. Dunn, Ivan J. Dmochowski, Jay R. Winkler,* and Harry B. Gray*

Contribution from the Beckman Institute, California Institute of Technology, Pasadena, California 91125

Received November 19, 2002; E-mail: hbgray@caltech.edu; winklerj@caltech.edu

Abstract: We report the synthesis and characterization of Ru-diimine complexes designed to bind to cytochrome P450cam (CYP101). The sensitizer core has the structure $[Ru(L_2)L']^{2+}$, where L' is a perfluorinated biphenyl bridge (F_8bp) connecting 4,4'-dimethylbipyridine to an enzyme substrate (adamantane, F_8bp-Ad), a heme ligand (imidazole, F_8bp-Im), or F (F_9bp). The electron-transfer (ET) driving force ($-\Delta G°$) is varied by replacing the ancillary 2,2'-bipyridine ligands with 4,4',5,5'-tetramethylbipyridine (tmRu). The four complexes all bind P450cam tightly: Ru$-F_8bp$-Ad (**1**, $K_d = 0.077\ \mu M$); Ru$-F_8bp$-Im (**2**, $K_d = 3.7\ \mu M$); tmRu$-F_9bp$ (**3**, $K_d = 2.1\ \mu M$); and tmRu$-F_8bp$-Im (**4**, $K_d = 0.48\ \mu M$). Binding is predominantly driven by hydrophobic interactions between the Ru-diimine wires and the substrate access channel. With Ru$-F_8bp$ wires, redox reactions can be triggered on the nanosecond time scale. Ru-wire **2**, which ligates the heme iron, shows a small amount of transient heme photoreduction (ca. 30%), whereas the transient photoreduction yield for **4** is 76%. Forward ET with **4** occurs in roughly 40 ns ($k_f = 2.8 \times 10^7\ s^{-1}$), and back ET (Fe$^{II} \rightarrow$ Ru^{III}, $k_b \approx 1.7 \times 10^8\ s^{-1}$) is near the coupling-limited rate (k_{max}). Direct photoreduction was not observed for **1** or **3**. The large variation in ET rates among the Ru-diimine:P450 conjugates strongly supports a through-bond model of Ru$-$heme electronic coupling.

Introduction

Electron transfer (ET) is often the rate-determining step in biological catalysis. The reactions of the cytochromes P450 are an excellent case in point.[1] In the archetypal P450 from *Pseudomonas putida* (P450cam), the natural redox partner, putidaredoxin (Putd), reduces the enzyme far too slowly ($k_{red} \approx 50\ s^{-1}$) to allow catalytic intermediates to accumulate under biological conditions (Scheme 1).[2]

We are studying a variety of Ru-diimine sensitizers designed to replace the slow biological reduction with a rapid optical redox trigger.[5,6] Each of the most promising sensitizers employs a perfluorobiphenyl group (F_8bp) that couples the Ru-diimine to a terminal functionality (Chart 1).

In these Ru-diimine:P450 conjugates, the Ru donor and the ferriheme acceptor are held in position mainly by noncovalent interactions. Thus, the synthetic flexibility of the sensitizer, together with the structural framework provided by the enzyme, makes this an ideal system for exploring basic ET parameters in a biologically relevant milieu.
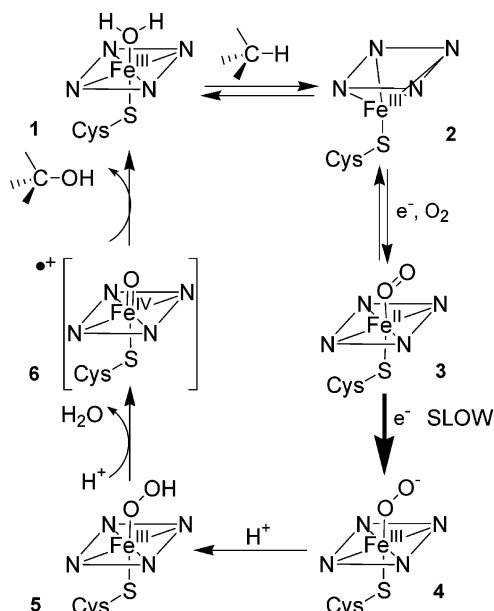
Experimental Section

General. P450cam and the mutant Y29F were expressed in *E. coli* and purified using standard procedures.[5,7] Site-directed mutagenesis was performed using Stratagene QuikChange mutagenesis kits. P450cam was stored in small aliquots and thawed immediately before use. Samples were prepared in 50 mM potassium phosphate buffer (pH 7.4) containing 100 mM KCl. P450 concentration was quantified using the heme Soret absorption at 416 nm ($\epsilon_{416} = 115\ mM^{-1}\ cm^{-1}$). All experiments were performed on samples with a ratio Abs$_{418}$/Abs$_{280} \geq$ 1.55 when camphor free. Spectroscopic experiments used custom quartz cuvettes fitted with Kontes Teflon stopcocks. Oxygen was removed from the sample by completing at least 30 cycles of partial vacuum followed by an influx of argon.

Absorption spectra were taken on an HP-8452A spectrophotometer. Steady-state luminescence spectra were taken on an ISS K2 fluorometer. Emission quantum yields were calculated relative to a Ru(bpy)$_3^{2+}$ standard, whose luminescence quantum yield was taken to be 0.042 in water.[8-10]
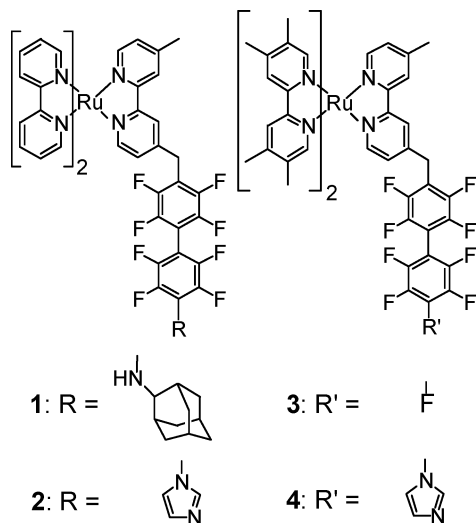
Reduction of P450cam. P450cam (5.1 μM) was reduced with sodium dithionite under an atmosphere of carbon monoxide in the presence of 1.2 equiv of tmRu$-F_8bp$-Im, producing the characteristic Soret peak at 446 nm. Carbon monoxide was then removed by gently bubbling argon through the sample for 5 min, resulting in both a change in shape and a decrease in intensity of the Soret peak (446 nm). This

(1) Ortiz de Montellano, P. R. *Cytochrome P450: Structure, Mechanism and Biochemistry*, 2 ed.; Plenum Press: New York, 1995; p 652.
(2) Fisher, M. T.; Sligar, S. G. *J. Am. Chem. Soc.* **1985**, *107*, 5018−5019.
(3) (a) Davydov, R.; Makris, T. M.; Kofman, V.; Werst, D. E.; Sligar, S. G.; Hoffman, B. M. *J. Am. Chem. Soc.* **2001**, *123*, 1403−1415. (b) Schlichting, I.; Berendzen, J.; Chu, K.; Stock, A. M.; Maves, S. A.; Benson, D. E.; Sweet, R. M.; Ringe, D.; Petsko, G. A.; Sligar, S. G. *Science* **2000**, *287*, 1615−1622.
(4) Groves, J. T.; McClusky, G. A.; White, R. E.; Coon, M. J. *Biochem. Biophys. Res. Commun.* **1978**, *81*, 154−160.
(5) Dmochowski, I. J.; Crane, B. R.; Wilker, J. J.; Winkler, J. R.; Gray, H. B. *Proc. Natl. Acad. Sci. U.S.A.* **1999**, *96*, 12987−12990.
(6) Wilker, J. J.; Dmochowski, I. J.; Dawson, J. H.; Winkler, J. R.; Gray, H. B. *Angew. Chem., Int. Ed.* **1999**, *38*, 90−92.

(7) Dmochowski, I. J. *Probing cytochrome P450 with sensitizer-linked substrates*; California Institute of Technology: Pasadena, CA, 2000, p 305.
(8) Roundhill, D. M. *Photochemistry and Photophysics of Metal Complexes*; Plenum Press: New York, 1994.
(9) van Houten, J.; Watts, R. J. *J. Am. Chem. Soc.* **1976**, *98*, 4853−4858.
(10) Cook, M. J.; Lewis, A. P.; McAuliffe, G. S. G.; Skarda, V.; Thomson, A. J.; Glasper, J. L.; Robbins, D. J. *J. Chem. Soc., Perkin Trans. 2* **1984**, 1293−1301.

Scheme 1 Cytochrome P450cam Catalytic Cycle[a]

[a] Upon binding, the substrate displaces water, converting the heme from 6-coordinate, low-spin **1** to 5-coordinate, high-spin **2**. Subsequent reduction by putidaredoxin produces the ferrous heme, which binds dioxygen (**3**). Reduction of **3** produces the ferrous, peroxide-bound heme (**4**), which rapidly protonates (**5**).[3] In the prevalent model, the peroxide then undergoes heterolysis to produce water and a ferryl [Fe^{IV}=O]$^{•+}$ species (**6**), which oxidizes the substrate.[4]

Chart 1. Ru-diimine Wires[a]

[a] **1** Ru−F$_8$bp-Ad; **2** Ru−F$_8$bp-Im; **3** tmRu−F$_9$bp; **4** tmRu−F$_8$bp-Im.

species was assigned as the imidazole-ligated ferrous heme, in agreement with the previously determined spectrum of *N*-phenylimidazole-ligated ferrous P450cam.[11] Subsequent addition of carbon monoxide to the cuvette resulted in the restoration of the Soret band of CO-ligated P450cam.

As a control, the same procedure was performed with 50 μM camphor replacing tmRu−F$_8$bp-Im. Five minutes of argon purging were sufficient to shift the Soret peak from 446 to 408 nm, indicative of complete conversion of CO-bound to five-coordinate ferrous heme.

Transient Spectroscopy. Transient absorption and emission data were collected using instruments described previously.[12,13] The instru-

(11) Dawson, J. H.; Andersson, L. A.; Sono, M. *J. Biol. Chem.* **1983**, *258*, 13637−13645.

ment possesses a response time of 20 ns (fwhm), and the data are digitized at 200 megasamples s^{-1}. For nanosecond luminescence decay measurements, the sample was excited at 10 Hz with 70-ps, 355-nm pulses from a regeneratively amplified mode-locked Nd: YAG laser. Luminescence from the cuvette was filtered with a 650-nm long-pass filter, collected directly by a fiber optic (Fiberguide Industries) and detected with a Hamamatsu C5680 streak camera. The data were recorded using Hamamatsu High Performance Digital Temporal Analyzer 3.1.0 software and fit using Microcal Origin 5.0.

Binding Constants. Luminescence decay profiles were fit to a biexponential function:

$$I(t) = c_1 e^{-k_1 t} + c_2 e^{-k_2 t} \qquad (1)$$

using nonlinear least squares with iterative reconvolution to account for finite instrument response. The ratio of enzyme-bound to free ruthenium complex is c_1/c_2, where k_1 and k_2 are the luminescence decay rate constants for the enzyme-bound and free ruthenium complexes.

This procedure has several advantages over steady-state UV−vis titrations. The absorption due to the ruthenium complexes complicates the determination of a dissociation constant from the direct titration of P450cam with a Ru-wire. Previous results have demonstrated that camphor and luminescent probe molecules may bind simultaneously to the enzyme, again complicating the derivation of dissociation constants from competition binding assays.[14]

Fitting errors for c_1, c_2, k_1, and k_2 were determined by systematically varying one parameter while optimizing the other three to minimize the sum of the absolute values of the difference between the model and the data. Limits on a particular variable were set when the presence of obvious residuals indicated that the model did not fit the data. In practice, the fitting error on c_1 and c_2 was found to be about 10% of the total amplitude: $\text{err}(c_1) = 0.1(c_1 + c_2)$. Propagation of this error through the determination of K_d, assuming the worst-case perfect correlation of c_1 and c_2, shows that the fitting error is 20% when $c_1 = c_2$, but becomes substantial when one phase predominates. For instance, when c_1 and c_2 account for 20 and 80% of the amplitude, the resulting K_d becomes uncertain to within a factor of 2.3.

ET Rate Constants. The raw transient absorption kinetics contain contributions from both heme/Ru redox processes and the bleach associated with the Ru-diimine excited state (*Ru^{2+}). The observed kinetics at 420 and 445 nm were corrected for the contribution of *Ru^{2+} prior to fitting. The *Ru^{2+} decay was recorded at 427 nm (the ferrous/ferric heme isosbestic). This trace was then scaled to account for the differences in *Ru^{2+}/Ru^{2+} extinction coefficients at 420, 427, and 445 nm (*Ru^{2+}/Ru^{2+} $\Delta\epsilon_{445}/\Delta\epsilon_{427} = 1.06$, $\Delta\epsilon_{420}/\Delta\epsilon_{427} = 0.83$) and subtracted from the kinetics at 420 and 445 nm.

Transient absorption kinetics were interpreted according to the model shown in Scheme 2. The change in optical density (ΔOD) at time t is given by eq 2:

$$(\Delta OD)(t) = \frac{k_f [^*Ru]_0 \Delta\epsilon}{k_b + k_{sep} - k_L} \left[\left(1 - \frac{k_{sep}}{k_L} \right) \exp(-k_L t) - \left(1 - \frac{k_{sep}}{k_b + k_{sep}} \right) \exp[-(k_b + k_{sep})t] + \frac{k_{sep}}{k_L} - \frac{k_{sep}}{k_b + k_{sep}} \right] \quad (2)$$

where $[^*Ru^{2+}]_0 (M^{-1})$ is the concentration of excited ruthenium complex at time zero and $\Delta\epsilon$ is the change in molar extinction coefficients:

(12) Dmochowski, I. J.; Winkler, J. R.; Gray, H. B. *J. Inorg. Biochem.* **2000**, *81*, 221−228.
(13) Low, D. W.; Winkler, J. R.; Gray, H. B. *J. Am. Chem. Soc.* **1996**, *118*, 117−120.
(14) Dunn, A. R.; Hays, A.-M. A.; Goodin, D. B.; Stout, C. D.; Chiu, R.; Winkler, J. R.; Gray, H. B. *J. Am. Chem. Soc.* **2002**, *124*, 10254−10255.

$$\Delta\epsilon(\lambda) = \epsilon_{Fe}^{II} - \epsilon_{Fe}^{III} + \epsilon_{Ru}^{III} - \epsilon_{Ru}^{II} \tag{3}$$

Sufficient laser power was used to ensure that all photosensitizer molecules were excited; $[*Ru^{2+}]_0 = [Ru]_{tot.}$. The values $\Delta\epsilon_{445} = 90$ mM^{-1} cm^{-1} and $\Delta\epsilon_{420} = -72$ mM^{-1} cm^{-1} were derived from the steady-state spectra of reduced and oxidized P450cam bound to tmRu–F$_8$bp-Im plus the known Ru^{II}/Ru^{III} $\Delta\epsilon$ values.[15,16] The rate constant $k_L(s^{-1})$ is the observed decay rate of $*Ru^{2+}$ in the presence of P450:

$$k_L = k_0 + k_f + k_E \tag{4}$$

where the other rate constants are for the intrinsic decay (k_0), forward electron transfer (k_f), and Förster energy transfer to the heme (k_E).

Because the rates of forward and back ET are comparable to the response time of our instrument, the instrumental response function was deconvolved from the observed kinetics.[17] The recorded ΔOD was converted into an intensity:

$$I = (I_0)(10^{-\Delta OD}) \tag{5}$$

The response function was then deconvolved from the observed intensity I by iterative reconvolution. The algorithm used was written in MatLab 5.3 and relies on the built-in simplex minimization algorithm.

Fitting errors for k_f, k_b, and k_{sep} were determined by systematically adjusting one variable while leaving the other two free to adopt whatever values minimized the sum of the absolute values of the difference between the model and the data. Limits on a particular variable were set when the presence of a clear residual indicated that the model did not fit the data. Error in the rates is best expressed as a multiplicative factor. The errors are estimated to be: k_f(445 nm) 2.1; k_f(420 nm) 1.8; k_b(445 nm) 2.3; k_b(420 nm) 2.0; k_{sep}(445 nm) 1.1; and k_{sep}(420 nm) 1.5. These errors are in accord with those expected for a multiexpontial fit to moderate quality data.[17]

Förster Energy Transfer. The rate constant k_E was calculated from standard theoretical expressions:[18]

$$k_E = k_0 \left(\frac{R_0}{r}\right)^6 \tag{6}$$

$$R_0^6 = 8.8 \times 10^{-5}(\kappa^2 n^{-4}\phi_0 J) \tag{7}$$

$$J = \frac{\int_0^\infty F_0(\lambda)E_A(\lambda)\lambda^4 \, d\lambda}{\int_0^\infty F_0(\lambda) \, d\lambda} \tag{8}$$
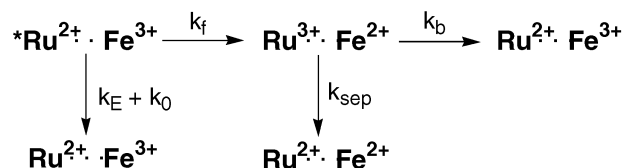
where J is the overlap between the luminescence spectrum of the donor and absorption spectrum of the acceptor (weighted by λ^4), ϕ_0 is the luminescence quantum yield in the absence of energy transfer, n is the index of refraction, and κ is an orientation factor dependent on the alignment of the donor and acceptor dipoles ($\kappa^2 = 2/3$ for random alignment).

Calculation of Buried Surface Area. The solvent-exposed surface areas of Ru–F$_8$bp-Ad, P450cam, and the P450cam:Ru–F$_8$bp-Ad conjugate (pdb code 1k2o) were calculated with the Solvation module of InsightII using a 1.4 Å probe. Buried surface area was computed by subtracting the surface area of the conjugate from that of Ru–F$_8$bp-Ad and P450cam alone. The difference in buried surface areas for the Δ and Λ stereoisomers of Ru–F$_8$bp-Ad is negligible.

Results

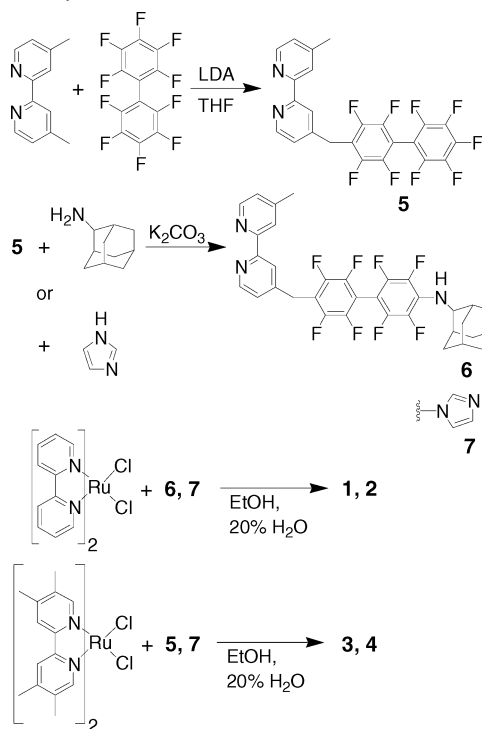**Synthesis.** Sequential nucleophilic substitution of decafluorobiphenyl proved to be an especially efficient route to the

(15) Kotkar, D.; Joshi, V.; Ghosh, P. K. *J. Chem. Soc., Chem. Commun.* **1987**, *1*, 4−6.
(16) Miller, R. R.; Brandt, W. W.; Puke, M. *J. Am. Chem. Soc.* **1955**, *77*, 3178−3180.
(17) Demas, J. N. *Excited State Lifetime Measurements*; Academic Press: New York, 1983.
(18) Wu, P.; Brand, L. *Anal. Biochem.* **1994**, *218*, 1−13.

Scheme 2. ET Processes in Photoexcited Ru-diimine:P450cam Conjugates[a]

[a] $*Ru^{2+}$ reduces the heme (k_f) or decays to the ground state through a combination of intrinsic decay (k_0) and energy transfer to the heme (k_E), which decays non-radiatively to the ground state. The charge-separated state (Ru^{3+}···Fe^{2+}) undergoes back electron transfer (k_b) or decays to form a long-lived ferrous heme (k_{sep}).[21]

Scheme 3. Synthesis of Ru-diimine Wires[a]

[a] Deprotonation of 4,4′-dimethyl-2,2′-bipyridine with lithium diisopropyl amide (LDA) followed by nucleophilic attack on decafluorobiphenyl results in the ET bridge **7**.

desired conjugated compounds (Scheme 3). Absorption and emission maxima at 456 and 620 nm (**1** and **2**) and 444 and 654 nm (**3** and **4**) are consistent with the previously reported spectra of [Ru(bpy)$_2$(Me$_2$bpy)]$^{2+}$ and [Ru(tmbpy)$_2$(bpy)]$^{2+}$.[19]

Binding. All of the Ru-diimine wires (**1–4**) bind to P450. Binding of Ru–F$_8$bp-Ad induces a shift in the Soret absorption maximum from 416 to 414 nm, consistent with partial displacement of water from the heme iron. Similarly, coordination of both Ru–F$_8$bp-Im and tmRu–F$_8$bp-Im shifts the Soret peak to 420 nm (Figure 1), consistent with the value of 421 nm reported for the ferric P450cam:*N*-phenylimidazole complex.[20] The measured extinction coefficient at 446 nm in the spectrum of the tmRu–F$_8$bp-Im:Fe^{II}-P450cam conjugate is 117 mM^{-1} cm^{-1}, in agreement with the value of 116 mM^{-1} cm^{-1} reported for the *N*-phenylimidazole complex.[11] All of the absorption spectra are consistent with predominantly low-spin hemes in the Ru-wire:P450cam conjugates.

(19) Opperman, K. A.; Mecklenburg, S. L.; Meyer, T. J. *Inorg. Chem.* **1994**, *33*, 5295−5301.
(20) Dawson, J. H.; Andersson, L. A.; Sono, M. *J. Biol. Chem.* **1982**, *257*, 3606−3617.
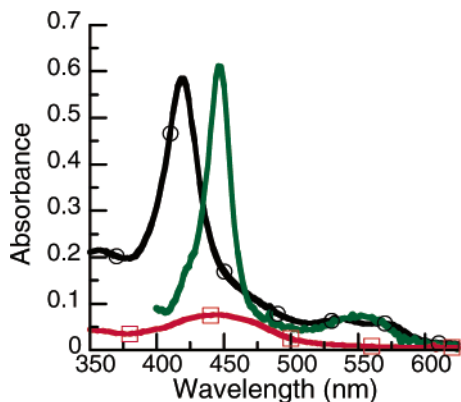
Figure 1. UV−vis absorption spectra of ferric P450cam (black, open circles), 5.2 μM tmRu−F$_8$bp-Im (red, open squares), and ferrous P450cam ligated by tmRu−F$_8$bp-Im (green).
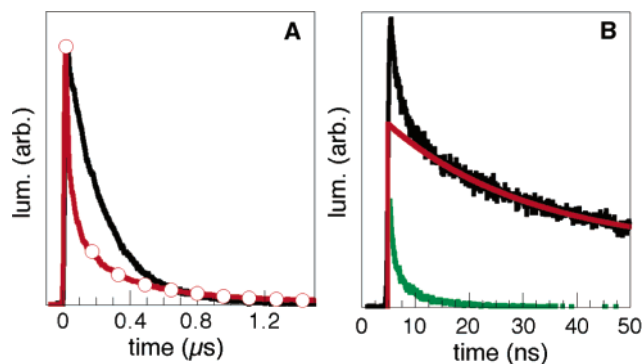

Figure 2. Luminescence decay. (A) 10 μM 1:1 tmRu−F$_8$bp-Im:P450cam luminescence decay (tmRu−F$_8$bp-Im, black; tmRu−F$_8$bp-Im + 1 equiv P450cam, red, open circles). (B) Nanosecond time scale luminescence decay of 1:1 tmRu−F$_8$bp-Im:P450cam (4.5 μM) (instrument response ca. 70 ps; see Experimental Section). The initial rapid ($k > 1 \times 10^9$ s^{-1}) decay is intrinsic to P450cam and likely represents a trace impurity. The slower decay on this time scale corresponds to the rapid decay in Figure 2A ($k_L = 3.7 \times 10^8$ s^{-1}). Green, P450cam; black, P450cam + tmRu−F$_8$bp-Im; red, monoexponential fit.

Table 1. Dissociation Constants

Ru-wire	μM[a]
Ru−F$_8$bp-Ad	0.077 ± 0.011
Ru−F$_8$bp-Im	3.7 ± 0.5
tmRu−F$_8$bp-Im	0.48 ± 0.18
tmRu−F$_9$bp	2.1 ± 1.3

[a] Uncertainties are standard deviations derived from independent analysis of at least three measurements.

All of the Ru-wires show biphasic luminescence decays in the presence of P450cam. The fast phase results from partial quenching due to energy transfer to the heme, and in the case of Ru−F$_8$bp-Im and tmRu−F$_8$bp-Im, electron transfer (see Scheme 2 and following sections). Although the heme Soret does not shift in the presence of tmRu−F$_9$bp, the biphasic luminescence decay of the Ru-wire due to energy transfer indicates that it too binds P450cam. Typical biphasic luminescence decays for a Ru-wire in the presence of P450 are shown in Figure 2. The ratio of the amplitudes of the fast (bound) and slow (free Ru-wire) phases was used to calculate binding constants (Table 1).

Electron Transfer. Upon 470-nm excitation, both tmRu−F$_8$bp-Im and Ru−F$_8$bp-Im reduce P450cam. The bleach at 420 nm and increase in optical density at 445 nm confirm the conversion of (^{Im}N)(^{Cys}S){^{Por}N$_4$Fe^{III}} to (^{Im}N)(^{Cys}S){^{Por}N$_4$Fe^{II}}
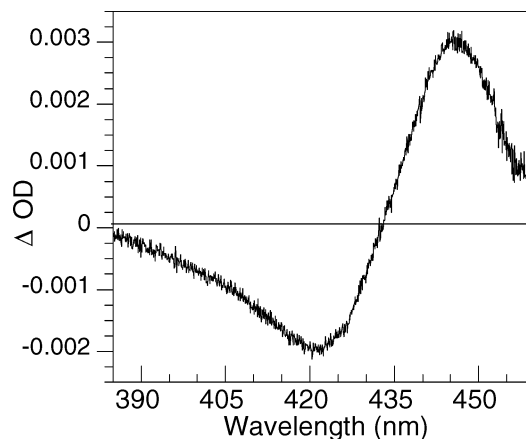

Figure 3. Transient absorption spectrum measured 20 μs after 470 nm excitation of equimolar tmRu−F$_8$bp-Im and P450cam (9.6 μM). Observed changes in optical density are chiefly due to the conversion of ferric to ferrous heme, with comparatively minor contributions from Ru^{II} to Ru^{III} oxidation.
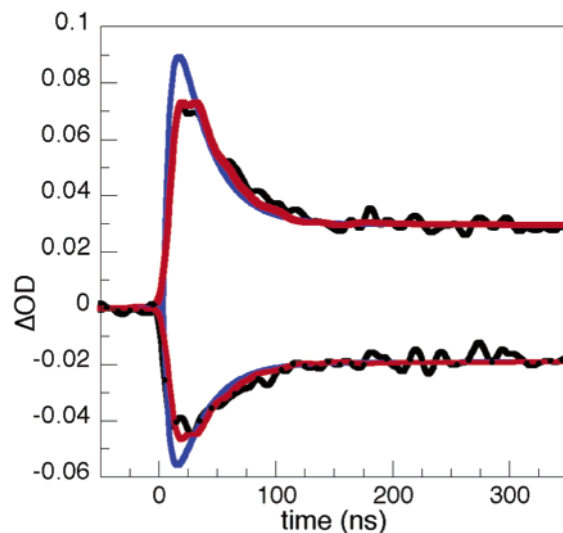

Figure 4. Transient absorption at 445 (top) and 420 nm (bottom) for 10 μM 1:1 tmRu−F$_8$bp-Im:P450cam (black, data; blue, fit; red, convolved fit). The kinetics were corrected for both free and bound *Ru^{2+} by measuring the transient absorption of *Ru^{2+} at a P450cam Fe^{II}/Fe^{III}, Ru^{II}/Ru^{III} isosbestic (427 nm). This spectrum was then scaled and subtracted from the kinetics recorded at 420 and 445 nm (Experimental Section). The data were fit to the kinetics model in Scheme 2 using iterative reconvolution to account for instrument response. The fit yielded the following rate constants: $k_f = 2.9 \times 10^7$, $k_b = 1.6 \times 10^8$, $k_{sep} = 8.6 \times 10^6$ s^{-1} (445 nm); and $k_f = 2.6 \times 10^7$, $k_b = 1.9 \times 10^8$, $k_{sep} = 9.3 \times 10^6$ s^{-1} (420 nm). The same procedure could not be applied to the transient absorption spectra of Ru−F$_8$bp-Im because the signal due to *Ru^{2+} is much larger than the signal due to the heme.

(Figure 3). Neither *Ru−F$_8$bp-Ad (***1**) nor *tmRu−F$_9$bp (***3**) reduces P450cam, as judged by the lack of a transient absorption signal.

Photoexcitation of equimolar tmRu−F$_8$bp-Im and P450cam shows complex early kinetics (Figure 4, Scheme 2). The sharp rise and fall at the beginning of the trace recorded at 445 nm are attributed to fast forward (k_f) and back (k_b) ET. The rates of accumulation and decay of Fe^{II} are comparable to the rise time of the instrument. Deconvolution was necessary to eliminate the instrument response contribution from the observed kinetics. Optimization of the parameters k_f, k_b, and k_{sep} at 420 and 445 nm yielded the following rate constants: $k_f = 2.8 \times 10^7$; $k_b = 1.7 \times 10^8$; $k_{sep} = 9.0 \times 10^6$ s^{-1}.[21]

Table 2. Derivation of k_f and Ru–Fe Distances from Luminescence Decay Measurements[a]

Ru-wire	$k_L \times 10^{-6}$ (s^{-1})	$k_0 \times 10^{-6}$ (s^{-1})	$k_E \times 10^{-6}$ (s^{-1})	$k_f \times 10^{-6}$ (s^{-1})	Ru–Fe (Å)	R_0 (Å)[b]
tmRu–F$_8$bp-Im	37	4.6	4.4[c]	28[d]	18.1[b]	18.0
Ru–F$_8$bp-Im	13	2.0	6.6[b]	4.4	18.1[e]	22.1
Ru–F$_8$bp-Ad	5.5	2.0	3.5[c]		22.1[b]	24.3
					cf. 21.8[f]	
tmRu–F$_9$bp	13	4.6	8.4[c]		17.0[b]	18.8

[a] Variation in R_0 stems from variation in the heme Q-bands and the emission spectrum of the complex. [b] Calculated from Förster theory (eqs 6–8). [c] $k_E = k_L - k_0 - k_f$. [d] From transient absorption kinetics. [e] In accord with the calculated Ru–Fe distance for tmRu–F$_8$bp-Im. [f] From the crystal structure of Ru–F$_8$bp-Ad:P450cam (ref 23).

In the absence of competing electron transfer (Ru–F$_8$bp-Ad and tmRu–F$_9$bp), the Ru–Fe distance can be calculated using Förster theory from k_E, the ruthenium emission spectrum, and the heme absorption spectrum (Table 2). The Ru–Fe distance (22.1 Å) calculated for Ru–F$_8$bp-Ad is in excellent agreement with the value from the crystal structure. The distance of 17 Å calculated for tmRu–F$_9$bp agrees well with structural modeling of the tmRu–F$_9$bp:P450cam conjugate and corresponds to a ~2 Å gap between the end of the perfluorinated biphenyl bridge and the heme.

Using eq 4, we calculated that k_E for tmRu–F$_8$bp-Im is 4.4 × 10^6 s^{-1} (Table 2). This rate of energy transfer corresponds to a Ru–Fe distance of 18.1 Å, a reasonable value given the geometric constraints of the fluorobiphenyl bridge. A Ru–Fe distance of 18.1 Å can in turn be used to calculate a k_E of 6.6 × 10^6 s^{-1} for Ru–F$_8$bp-Im, corresponding to $k_f = 4.4 \times 10^6$ s^{-1}, which is 6 times slower than photoinduced reduction of ferric P450cam by tmRu–F$_8$bp-Im. With $\phi = (k_f/k_L)$, we find total ferrous heme yields of 76% for tmRu–F$_8$bp-Im and roughly 30% for Ru–F$_8$bp-Im.

Discussion

The observed binding constants suggest that the interaction between the ruthenium complex and the enzyme is primarily hydrophobic in nature. Ru–F$_8$bp-Ad, which has the largest hydrophobic surface area, binds best, and tmRu–F$_8$bp-Im binds better than its nonmethylated analogue Ru–F$_8$bp-Im. Previous work suggests that the binding energy derived from burying hydrophobic surfaces is around 15 cal Å^{-2} for protein–protein interactions.[22] The crystal structure of Ru–F$_8$bp-Ad bound to P450cam shows extensive contacts between the Ru-wire and the hydrophobic substrate access channel,[23] resulting in 1.2 × 10^3 Å^2 of buried surface area (Figure 5), corresponding to 8.2

(21) Although most of the photoproduced ferrous heme decays in 50 ns, a small percentage remains. The Soret maximum at 445 nm is observed on all the time scales we can measure, suggesting that dissociation does not explain the long-lived charge-separated state. The mutations Y29F and Y96A do not affect the observed kinetics, indicating that the transiently generated Ru(bpy)$_3$$^{3+}$ does not oxidize these nearby residues. Tyrosine oxidation by Ru-diimine complexes has been previously observed: (a) Sjodin, M.; Styring, S.; Åkermark, B.; Sun, L. C.; Hammarström, L. *J. Am. Chem. Soc.* **2000**, *122*, 3932–3936. (b) Magnuson, A.; Berglund, H.; Korall, P.; Hammarström, L.; Akermark, B.; Styring, S.; Sun, L. C. *J. Am. Chem. Soc.* **1997**, *119*, 10720–10725. Several studies have shown that [Ru-(bpy)$_3$]$^{3+}$ decays through multiple pathways in aqueous solution: (a) Brune, S. N.; Bobbitt, D. R. *Talanta* **1991**, *38*, 419–424. (b) Ledney, M.; Dutta, P. K. *J. Am. Chem. Soc.* **1995**, *117*, 7687–7695. (c) Ghosh, P. K.; Brunschwig, B. S.; Chou, M.; Creutz, C.; Sutin, N. *J. Am. Chem. Soc.* **1984**, *106*, 4772–4783. (d) Arce-Sagues, J. A.; Gillard, R. D.; Lancashire, R. J.; Williams, P. A. *J. Chem. Soc., Dalton Trans.* **1979**, *1*, 193–198. (e) Creutz, C.; Sutin, N. *Proc. Natl. Acad. Sci. U.S.A.* **1975**, *72*, 2858–2862. The yield of reduced P450 at 5 μs is about 1.7% for tmRu–F$_8$bp–Im and 0.5% for Ru–F$_8$bp–Im, as judged by transient absorption at 445 nm. Thus, the processes leading to the long-lived ferrous heme constitute a minor side reaction compared to the initial forward and back electron transfer.

(22) Eisenberg, D.; McLachlan, A. D. *Nature* **1986**, *319*, 199–203.

(23) Dunn, A. R.; Dmochowski, I. J.; Bilwes, A. M.; Gray, H. B.; Crane, B. R. *Proc. Natl. Acad. Sci. U.S.A.* **2001**, *98*, 12420–12425.
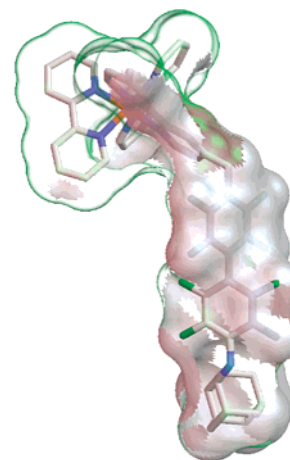
Figure 5. The Ru–F$_8$bp-Ad wire is partially buried upon binding to P450cam. The buried surface (gray, 56% of the total surface area) was computed with the program GRASP using a 1.4 Å radius probe.
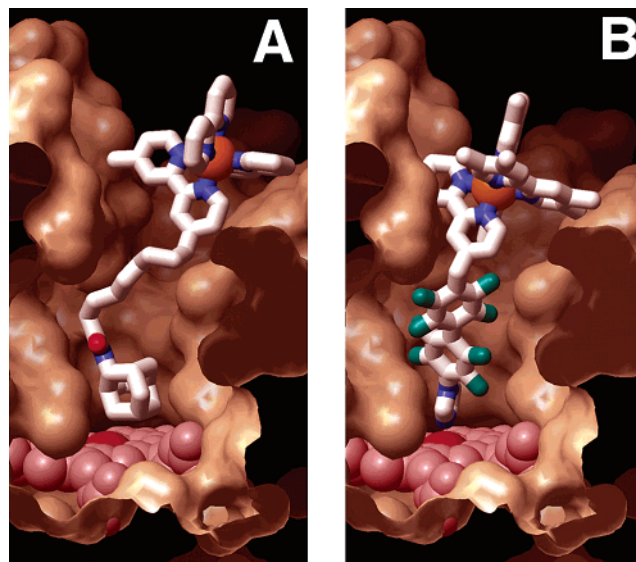

Figure 6. (A) Cutaway view of the 1.55 Å resolution crystal structure of [Ru–C$_9$-Ad]$^{2+}$ bound to P450cam.[20] Photochemically generated [Ru–C$_9$-Ad]$^+$ reduces ferric P450cam with a time constant of about 50 μs ($-\Delta G° \approx 1.0$ eV).[6] (B) tmRu–F$_8$bp-Im modeled into the active site of P450cam. The perfluorobiphenyl bridge improves the electronic coupling between *Ru^{2+}(L$_2$)L′ and the heme, resulting in direct photoreduction with a time constant of 36 ns even at lower driving force ($-\Delta G° \approx 0.45$ eV).

cal Å^{-2}. A similar calculation based on the crystal structure of Ru–C$_9$-Ad bound to P450cam (Figure 6) yields similar binding energies (Δ isomer: 9.13 kcal mol^{-1}, 8.4 cal Å^{-2}; Λ isomer: 9.69 kcal mol^{-1}, 9.3 cal Å^{-2}).[12] The gain in binding for hydrophobic burial is lower for our complexes than that observed at protein interfaces. In part this result must reflect the energetic cost of "opening" the enzyme.[23]

Table 3. Reduction Potentials

redox couple	potential (V, NHE)
P450cam (Fe$^{3+/2+}$)	$\sim-0.3^{a}$
[Ru(bpy)$_3$]$^{3+/2+*}$	-0.62^{b}
[Ru(tmbpy)$_3$]$^{3+/2+*}$	-0.75^{c}
[Ru(bpy)$_3$]$^{3+/2+}$	1.26^{b}
[Ru(tmbpy)$_2$(dmbpy)]$^{3+/2+}$	1.07^{d}

^{a} Low spin (ref 35). ^{b} Reference 8. ^{c} Reference 36. ^{d} In MeCN vs SSCE (ref 19).

The imidazole-functionalized complexes weakly ligate the ferric heme, as tmRu−F$_8$bp-Im binds with only 0.87 kcal mol^{-1} greater affinity than tmRu−F$_9$bp. The small energetic contribution of coordination may result from steric effects or poorer σ-donating ability stemming from the electron-withdrawing perfluorobiphenyl unit.

These results and previous work[14] suggest that designing a small molecule to bind in a given enzyme active site can be relatively straightforward. Hydrophobic interactions are nondirectional, predictable, and hence easily engineered: 1000 Å^2 of buried surface area should result in a low micromolar dissociation constant. Of course, this simple strategy does not include considerations such as target specificity or water solubility, two important qualities in drug design.

ET Kinetics. According to semiclassical theory, coupling-limited electron tunneling (k_{max}) will occur when the driving force ($-\Delta G°$) equals the reorganization energy (λ).[24,25] Back electron transfer in the P450cam:tmRu−F$_8$bp-Im conjugate ($-\Delta G° \approx 1.5$ eV) should be in the inverted region for λ in the range 0.7−0.9 eV; the reaction should be 10 ($\lambda = 0.9$ eV) to 5000 ($\lambda = 0.7$ eV) times slower than forward electron transfer.[26] The inverted effect has been observed in several biological[27] and synthetic ET systems.[28] We found, however, that back ET is 10 times faster than the forward reaction. One possible explanation is that electron transfer initially produces an electronically excited product;[29,30] another is phonon-modified inelastic tunneling, which can be activationless in the classical inverted region.[31]

The transient absorption data show that tmRu−F$_8$bp-Im injects electrons into the ferriheme of P450cam more efficiently than Ru−F$_8$bp-Im. The methyl groups in tmRu−F$_8$bp-Im increase the driving force for forward electron transfer by

0.13 eV (Table 3). Semiclassical theory predicts a 4-fold increase in the rate of forward electron transfer, in qualitative agreement with the ET rates calculated from transient absorbance and luminescence decay rates (Table 2).

Structural variations in the Ru-wires allowed us to test the role of the intervening medium on the rate of electron transfer. Taking into account the differences in Ru−heme distances and driving forces, a coupling model with a uniform distance decay[32] of 1.1 Å^{-1} and $\lambda = 0.8$ eV[27a,30] predicts only 12-fold faster ET for tmRu−F$_8$bp-Im compared to Ru−C$_9$-Ad, instead of the 1400-fold rate difference that is observed (Figure 6). Similarly, tmRu−F$_8$bp-Im efficiently reduces P450cam while tmRu−F$_9$bp does not, despite the similarity in donor−acceptor distances and driving forces. The saturated bonds in Ru−C$_9$-Ad and the through-space jump in tmRu−F$_9$bp likely weaken electronic couplings compared to those associated with the imidazole-terminated Ru-wires and, hence, greatly slow ET.[33] Our results thus strongly support a through-bond model for coupling the Ru and heme centers.[34]

The biological reduction of P450cam by Putd (50 s^{-1}) is slow for two reasons: the driving force is low and the coupling to the deeply buried heme is weak. The coupling to the ferriheme was enhanced in enzyme conjugates containing the first generation of ruthenium sensitizer-linked substrates, which featured a direct ET pathway through a saturated alkyl chain. As a result, ET occurs on a submillisecond time scale (2 × 10^4 s^{-1}).[6] Both theory and experiment indicate that incorporating aromatic groups into the linker will further enhance the electronic coupling.[37] By employing a more direct, largely conjugated path, tmRu−F$_8$bp-Im is able to photoreduce P450cam in nanoseconds (2.8 × 10^7 s^{-1}), 10^3 times faster than the Ru-wire with an alkyl chain linker and 5 × 10^5 times faster than putidaredoxin.

Concluding Remarks

Photoreduction of the enzyme by the channel-specific Ru−imidazole wires occurs on the nanosecond time scale, fully 5 orders of magnitude faster than reduction by the natural redox partner putidaredoxin. Fast electron injection was only observed in the imidazole-terminated Ru-wires. However, calculations based on simple electronic coupling models suggest that

(24) Marcus, R. A. *J. Chem. Phys.* **1956**, *24*, 966−989.
(25) Marcus, R. A.; Sutin, N. *Biochim. Biophys. Acta* **1985**, *811*, 265−322.
(26) We assume that $\lambda_{Ru} = 0.57$ eV and λ_{heme} falls between 0.7 and 1.2 eV (Winkler, J. R.; Wittung-Stafshede, P.; Leckner, J.; Malmström, B. G.; Gray, H. B. *Proc. Natl. Acad. Sci. U.S.A.* **1997**, *94*, 4246−4249).
(27) (a) Scott, J. R.; Willie, A.; McLean, M.; Stayton, P. S.; Sligar, S. G.; Durham, B.; Millett, F. *J. Am. Chem. Soc.* **1993**, *115*, 6820−6824. (b) Turro, C.; Zaleski, J. M.; Karabatsos, Y. M.; Nocera, D. G. *J. Am. Chem. Soc.* **1996**, *118*, 6060−6067.
(28) (a) Gould, I. R.; Moser, J. E.; Armitage, B.; Farid, S.; Goodman, J. L.; Herman, M. S. *J. Am. Chem. Soc.* **1989**, *111*, 1917−1919. (b) Wasielewski, M. R.; Niemczyk, M. P.; Svec, W. A.; Pewitt, E. B. *J. Am. Chem. Soc.* **1985**, *107*, 1080−1082. (c) Ohno, T.; Yoshimura, A.; Mataga, N. *J. Phys. Chem.* **1986**, *90*, 3295−3297. (d) Chen, P.; Duesing, R.; Tapolsky, G.; Meyer, T. J. *J. Am. Chem. Soc.* **1989**, *111*, 8305−8306. (e) Closs, G. L.; Miller, J. R. *Science* **1988**, *240*, 440−447. (f) Fox, L. S.; Kozik, M.; Winkler, J. R.; Gray, H. B. *Science* **1990**, *247*, 1069−1071.
(29) Beitz, J. V.; Miller, J. R. *J. Chem. Phys.* **1979**, *71*, 4579−4595.
(30) (a) Mines, G. A.; Bjerrum, M. J.; Hill, M. G.; Casimiro, D. R.; Chang, I.-J.; Winkler, J. R.; Gray, H. B. *J. Am. Chem. Soc.* **1996**, *118*, 1961−1965. (b) Makinen, M. W.; Churg, A. K. Structural and analytical aspects of the electronic spectra of heme proteins. In *Iron Porphyrins*; Lever, A. B. P., Gray, H. B., Eds.; Addison-Wesley: Reading, MA, 1983; Vol. 1, pp 141−236.
(31) Daizadeh, I.; Medvedev, E. S.; Stuchebrukhov, A. A. *Proc. Natl. Acad. Sci. U.S.A.* **1997**, *94*, 3703−3708.

(32) Langen, R.; Colon, J. L.; Casimiro, D. R.; Karpishin, T. B.; Winkler, J. R.; Gray, H. B. *J. Biol. Inorg. Chem.* **1996**, *1*, 221−225.
(33) Beratan, D. N.; Skourtis, S. S. *Curr. Opin. Chem. Biol.* **1998**, *2*, 235−243.
(34) (a) Winkler, J. R. *Curr. Opin. Chem. Biol.* **2000**, *4*, 192−198. (b) Onuchic, J. N.; Beratan, D. N.; Winkler, J. R.; Gray, H. B. *Annu. Rev. Biophys. Biomol. Struct.* **1992**, *21*, 349−377. (c) Beratan, D. N.; Onuchic, J. N.; Winkler, J. R.; Gray, H. B. *Science* **1992**, *258*, 1740−1741.
(35) (a) Gunsalus, I. C.; Meeks, J. R.; Lipscomb, J. D. *Ann. N.Y. Acad. Sci.* **1973**, *212*, 107−121. (b) Sligar, S. G.; Gunsalus, I. C. *Proc. Natl. Acad. Sci. U.S.A.* **1976**, *73*, 1078−1082.
(36) Elliott, C. M.; Freitag, R. A.; Blaney, D. D. *J. Am. Chem. Soc.* **1985**, *107*, 4647−4655.
(37) (a) Smalley, J. F.; Feldberg, S. W.; Chidsey, C. E. D.; Linford, M. R.; Newton, M. D.; Liu, Y.-P. *J. Phys. Chem.* **1995**, *99*, 13141−13149. (b) Warman, J. M.; Smit, K. J.; de Haas, M. P.; Jonker, S. A.; Paddon-Row, M. N.; Oliver, A. M.; Kroon, J.; Oevering, H.; Verhoeven, J. W. *J. Phys. Chem.* **1991**, *95*, 1979−1987. (c) Langen, R.; Chang, I.-J.; Germanas, J. P.; Richards, J. H.; Winkler, J. R.; Gray, H. B. *Science* **1995**, *268*, 1733−1735. (d) Creager, S.; Yu, C. J.; Bamdad, C.; O'Connor, S.; MacLean, T.; Lam, E.; Chong, Y.; Olsen, G. T.; Luo, J. Y.; Gozin, M.; Kayyem, J. F. *J. Am. Chem. Soc.* **1999**, *121*, 1059−1064. (e) Sikes, H. D.; Smalley, J. F.; Dudek, S. P.; Cook, A. R.; Newton, M. D.; Chidsey, C. E. D.; Feldberg, S. W. *Science* **2001**, *291*, 1519−1523. (f) Pollard, W. T.; Felts, A. K.; Friesner, R. A. *Adv. Chem. Phys.* **1996**, *93*, 77−134. (g) Davis, W. B.; Wasielewski, M. R.; Ratner, M. A.; Mujica, V.; Nitzan, A. *J. Phys. Chem. A* **1997**, *101*, 6158−6164. (h) McConnell, H. M. *J. Chem. Phys.* **1961**, *35*, 508−515.

improved conjugation could overcome the loss of a direct bond to the heme.[33]

Hydroxylation catalyzed by P450cam is only one example of numerous biological processes, including photosynthesis and respiration, that involve oxidation and reduction steps. Current methods for studying enzyme reactions, for instance, stopped-flow mixing and photocaged substrates, have time resolutions limited by diffusion. Intramolecular ET in Ru-substrate:enzyme conjugates dramatically improves the accessible time resolution.

Supporting Information Available: Synthesis and characterization of Ru-diimine complexes (PDF). This material is available free of charge via the Internet at http://pubs.acs.org.

JA0294111